Numerical simulation of chicken manure gas reformers using an extended chemical reaction mechanism

M. Abou-Ellail[1], R. Amano[1] & K. Beshay[2]
[1]*Mechanical Engineering Department,*
University of Wisconsin-Milwaukee, USA
[2]*Mechanical Engineering Department, Cairo University, Egypt*

Abstract

The present paper is concerned with the numerical computations of flow, heat transfer and chemical reactions in two-dimensional cylindrical gas reformers. The reformer is overlaid with a two-dimensional grid of nodes having 300 in the radial direction and 1000 nodes in the axial direction. The governing equations for momentum, mass continuity, energy and species mass fractions are solved numerically using finite-volume procedures. The solutions are considered converged when the errors in the finite-volume equations are less than 0.1 percent. The reformer is fed with gasified gas coming from the gasifier at temperatures ranging from 1000 K to 1300 K. Moreover, the reformer is also supplied with hot air at temperatures ranging from 700 K to 800 K. The reformer diameter is 350 mm and is 4574 mm high. The reformed gases contain air, methane, hydrogen, nitrogen, carbon monoxide and carbon dioxide. The volume flow rates of the gasified gas range between 60 and 80 Nm^3/s. However, the hot air volume flow rates range between 20 and 30 Nm^3/s. The obtained results for the gas reformer performance at different operating conditions are compared with the limited available experimental data for similar reformers. The agreement is acceptable with some discrepancies in the compositions of the gases exiting the reformer. This is because some of the geometries and boundary conditions of the tested gas reformers are missing.

Keywords: numerical simulation, gas reformer, chemical reactions, species mole fraction.

WIT Transactions on Engineering Sciences, Vol 68, © 2010 WIT Press
www.witpress.com, ISSN 1743-3533 (on-line)
doi:10.2495/HT100081

1 Introduction

In the poultry industry, both growers and integrators are concerned that increasingly stringent environmental policies governing litter management will add expense and decrease an already slim profit margin, or that these factors could make poultry production unprofitable for some producers. To address these concerns, the poultry industry has recently begun considering, and in a few instances pursuing, large-scale, centralized litter processing (e.g., pellet-production and/or cogeneration) as alternative litter management strategies. However, such approaches involving large-scale, centralized facilities have several disadvantages, including high capital and operating costs, increased use of non-renewable energy for transportation and pellet-production, small added value, concern for the spread of pathogens during raw litter transportation, litter availability and supply issues, and complex just-in-time management required to keep a large-scale process at economic capacity [1].

Recently, efforts have been devoted to developing farm-scale litter management schemes that may have positive economic benefits for the poultry farmer when utilized in small modular systems, including farm-scale gas production modules that fuel furnaces and brooders in a poultry house and that fuel combined heat and power systems. The farm-scale approach benefits from economies of mass production, low capital costs, simple on-farm litter management, no feedstock supply limitations, zero transportation costs, and pathogen sterilization before exporting the recovered ash to commercial fertilizer markets elsewhere [2, 3].

Such units were built commercially by Yoshikawa and Hara [4], Yoshikawa [5] and Min and Yoshikawa [6]. Figure 1 shows the block-flow diagram of the commercial plant. The gasification and reforming units consist of a fixed-bed type up-draft gasifier and a reformer. The chicken manure dried in the dryer is supplied from the top of the gasifier by the continuous feeding system and the ash is extracted from the bottom of the gasifier. The gasification agent (air +

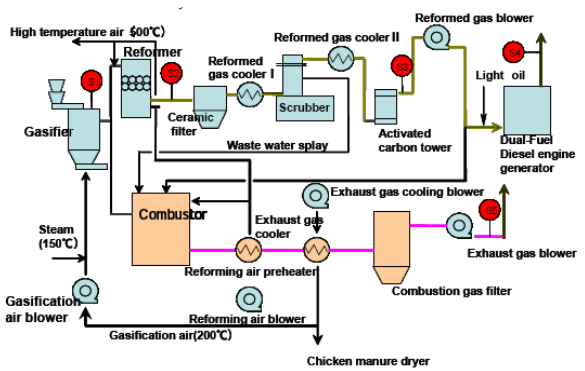

Figure 1: Block-flow diagram of the gasification and power generation system [4].

steam) is preheated up to 200°C and is supplied from the bottom of the gasifier. The tar contained in the pylorysis gas is decomposed into inflammable gases without catalyst under the action of high temperature air preheated to 500°C in the reformer. The reforming reaction is accelerated in the pebble layer, which is composed of packed ceramic balls of 30-mm in diameter and is located about 600 mm downstream from the reformer inlet. The remaining dust in the reformed gas is removed by the high temperature dust filter. The reformed gas is then cooled in the gas cooler generating the condensate. The condensate is stored in the drain drum, and is sprayed into the combustor. Therefore, this facility does not need a waste water treatment unit. Detrimental gas components in the reformed gas are removed by the activated carbon sucker tower and the reformed gas is supplied through the exhaust gas blower to the dual-fueled diesel engine generator. On the other hand, the excess gas coming out of the gasifier is burned in the combustor and is used to preheat the air for reforming. The condensed water recovered in the reformed gas coolers is atomized into the combustor for evaporation purposes. Therefore, no waste water treatment system was required.

A complete and comprehensive modeling of such systems would require dealing with the gasifier and reformer. The present paper handles predictions of the detailed flow and chemical reactions that take place in the reformer, while that in the gasifier will be covered in future work. A multi-step reaction mechanism is adopted. It involves 52 elementary reactions and 16 chemical species for methane/air mixtures [7].

2 Mathematical model

The governing equations for laminar reacting flows in the reformer containing a layer of packed ceramic balls are presented in this section.

2.1 Continuity and momentum equations

The mass continuity of reacting flow may be written as:

$$\frac{\partial(\rho\varepsilon)}{\partial t}+\frac{\partial(\varepsilon\rho u_i)}{\partial x_i}=0 \tag{1}$$

The momentum equation for laminar reacting flow may be written in Cartesian tensor notations as [8]:

$$\frac{\partial\left(\rho\varepsilon u_j\right)}{\partial t}+\frac{\partial}{\partial x_i}\left(\rho\varepsilon u_j u_i\right)-\frac{\partial}{\partial x_i}\left(\rho\varepsilon\upsilon\frac{\partial u_j}{\partial x_i}\right)=-\frac{\partial(\varepsilon P)}{\partial x_j}+\frac{\partial}{\partial x_i}\left[\rho\varepsilon\upsilon\left(\frac{\partial u_i}{\partial x_j}-\frac{2}{3}\frac{\partial u_k}{\partial x_k}\delta_{ij}\right)\right]-\frac{\mu\varepsilon^2}{K}u_j \tag{2}$$

where ρ is the gas density; ε is the porosity of the ceramic layer; u_j is the gas velocity along coordinate x_j; ν and μ are the kinematic and dynamic viscosities; K is the porous media permeability. The last term on the right-hand-side of

Equation (2) is the Darcy resistance to the flowing gas through the pores of the porous media. Equations (1) and (2) can also be applied to the flow of gases beyond the porous burner where ε is unity and K is assigned an infinitely large number to remove the last term of Equation (2).

2.2 Energy equations

The energy equation for the flow in the reformer is written as:

$$\frac{\partial(\rho\varepsilon h_g)}{\partial t}+\frac{\partial}{\partial x_i}\left(\rho\varepsilon u_i h_g\right)-\frac{\partial}{\partial x_i}\left(\Gamma_h\varepsilon\frac{\partial h_g}{\partial x_i}\right)= -\varepsilon\sum_j\left(\Delta H_j\right)W_j+(1-\varepsilon)ha(T_s-T_g) \tag{3}$$

Where, h_g is the gas sensible enthalpy; Γ_h is the thermal diffusivity; ΔH_j and W_j are the enthalpy of reaction and reaction rate of chemical reaction j of the reaction mechanism involving methane-air mixtures. The heat transfer coefficient between the gas and the solid is h while a is the surface area of the solid particles per unit volume of the solid [7]; (1-ε) is needed in the gas-solid heat exchange term to modify it to source term per unit combined volume of gas and solid consistent with the control volume of the rest of terms in Equations (3) and (4); T_g, T_s and k_s are the gas temperature, solid temperature and the solid thermal conductivity, respectively. It should be mentioned that the gas flow outside the porous layer, ε =1 and hence the heat exchange term vanishes from Equation (3). In the above equations, the subscripts s and g denote solid and gas respectively. The gas temperature, at any point, is directly related to the local gas sensible enthalpy (h_g), gas species mass fractions (Y_l) and constant-pressure specific heats.

2.3 Species mass fraction equations

The species mass fraction for reacting flow in the reformer may be written as:

$$\frac{\partial(\rho\varepsilon Y_l)}{\partial t}+\frac{\partial\left(\rho\varepsilon u_i Y_l\right)}{\partial x_i}-\frac{\partial}{\partial x_i}\left(\varepsilon\Gamma_{Y_l}\frac{\partial Y_l}{\partial x_i}\right)=\varepsilon M_l\sum_m\nu_{lm}W_m \tag{4}$$

Where, Y_l is the mass fraction of species l while Γ_{Yl} is its molecular diffusivity; M_l is the molecular mass of species l; ν_{lm} is the stoichiometric coefficient of species l in reaction m while W_m is the reaction rate of the elementary chemical reaction m of the reaction mechanism. It consists of 49 elementary reactions. The chemical kinetic mechanism involves 16 species, namely, CH_4, CH_3, CH_2, CH, CH_2O, CHO, CO, CO_2, O_2, O, OH, H, H_2, H_2O, HO_2 and H_2O_2 [7]. It should be mentioned here that ν_{lm} is taken as a positive value for products and negative for reactants as required for proper summation of the effect of each reaction on the production of a particular species. Although the above governing equations are written in Cartesian tensor notations, their cylindrical-polar counterparts are solved here for the axisymmetric porous burner of Figure 1. Moreover, the

unsteady terms of the above equations were not considered as the present porous burner is working under steady-state condition.

3 Solution procedure

The governing equations for heat, mass and momentum transfer can be written in a general form, as follows [8, 9]

$$\frac{\partial(\varepsilon\rho\psi)}{\partial t}+\frac{\partial(\varepsilon\rho u_i\psi)}{\partial x_i}-\frac{\partial}{\partial x_i}(\varepsilon\Gamma_\psi\frac{\partial\psi}{\partial x_i})=S_\psi \tag{5}$$

where ψ stands for u_j, gas sensible enthalpy, species mass fractions Y_l and pressure correction p'.

The axisymmetric flow domain (reformer) is overlaid with a finite grid of nodes. At each nodal point, the cylindrical-polar counterpart of the general governing equation (Equation (5)) is formally integrated over a control volume surrounding this nodal point. The formal integration is performed with due care to preserve the physical meaning and overall balance of each dependent variable. The final form of the finite difference equations are written as follows [8]:

$$(\Sigma(a_n) - S_p)\,\psi_p = \Sigma\,(a_n\,\psi_n) + S_u \tag{6}$$

where, ψ stands for any of the dependent variables, namely, axial and radial velocity components (u, v),gas sensible enthalpy, solid temperature, species mass fractions, or the pressure correction which is used to satisfied both mass continuity and momentum equations simultaneously. The summation (Σ) is over the four neighbors' n of a typical node p. The above finite difference coefficients are computed using the upwind method, such that these coefficients are always non-negative to give the proper combined effects of convection and diffusion.. Sp and Su are the coefficients of the integrated source term over the control volume surrounding node p. The pressure correction equation, which is a modified form of the mass continuity equation, is a Poisson –type equation that require special treatment of boundary conditions [8].

The solution procedure is based on the line-by-line alternating direction TDMA algorithm [8]. The difference equations (Equation (6)) for each dependant variable are modified at the outer boundary conditions of the reformer, to impose the conditions there. At the solid walls, the velocity components vanish while all other dependent variables normal gradients equal to zero. Similarly, along the centerline except that here only the radial velocity is equal to zero. At the exit section, all variables radial gradients are equal to zero, except for the pressure correction, which is zero itself. This is based on pre-specified pressure at exit, which allows the radial velocity to adjust according to the pressure gradient across the exit section. The inlet condition is specified for all dependent variables as given in the next section. The solution is then obtained using the above algorithm. The solution is then repeated for all the dependant variables.

4 Presentation and discussion of results

The present numerical simulations are performed for the reformer used by Yoshikawa and Hara [4]. The reformer geometry is depicted in Fig. 2. The reformer has a cylindrical shape of diameter 350 mm and height 5674 mm. Gas from the gasifier (contains H_2, CO, CH_4, N_2 and CO_2) is fed to the reformer at the top through a cylindrical inlet of diameter 100 mm, at a speed of 600 cm/s and a temperature of 1173 K. The mole fraction of the inlet gases are 0.065, 0.22, 0.013, 0.534 and 0.082 for H_2, CO, CH_4, N_2 and CO_2 respectively. Hot air is also fed to the reformer at the annulus surrounding the gas coming from the gasifier, at a speed of 15 cm/s and a temperature of 774 K. The reformer in the experimental work [4] is equipped with a layer of packed ceramic balls. It should be mentioned here that such ceramic layer is not taken into consideration in the present work, although the equations contain the parameters concerning porous media which will be necessary for future investigation. Due to the symmetry around the reformer centerline, only one half of the reformer is considered. The reformer is overlaid with a two-dimensional axisymmetric grid of nodes having 300 nodes in the radial direction and 1000 nodes in the axial direction. The governing equations of momentum, mass continuity, energy and species mass fractions are solved numerically using finite-volume procedures. The solutions are considered converged when the errors in the finite-volume are less than 0.1 percent.

The predicted mole fractions of the different species encountered in the reaction mechanism are given as a radial profiles at some specified axial locations. These locations are chosen to represent the inlet section (X=1cm), one

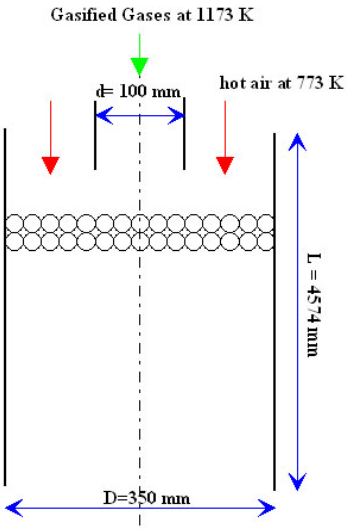

Figure 2: Layout of the reformer.

fourth of the reformer height (X = 88 cm), half the height (X = 188 cm) and after the exit section of the reformer (X = 580 cm). The predicted radial distributions of O_2 and H_2 are depicted in Fig. 3. Hydrogen at entry is confined to the inlet of the reformer (coming from the gasifier), while the oxygen as expected is confined to the annulus surrounding this entry. As the exit section of the reformer is approached, both gas steams diffuse into each other and chemical reactions occur at the prevailing temperature to produce the shown trend. The axial distribution of the mole fraction is then plotted at the centerline of the reformer as shown in Fig. 4. The observed increase in O_2 mole fraction at the centerline of the reformer exit is attributed mainly to the mixing of the air with the rest of the gasified gases while the increase in H2 mole fraction is attributed to the possible reversible reactions of the reaction species.

The average mole fraction of the reformed gases at the exit section can be calculated from the following equation

$$\overline{\varphi} = \frac{\int_0^{r_o} r\,\rho u \varphi\, dr}{\int_0^{r_o} r\,\rho u\, dr} \tag{7}$$

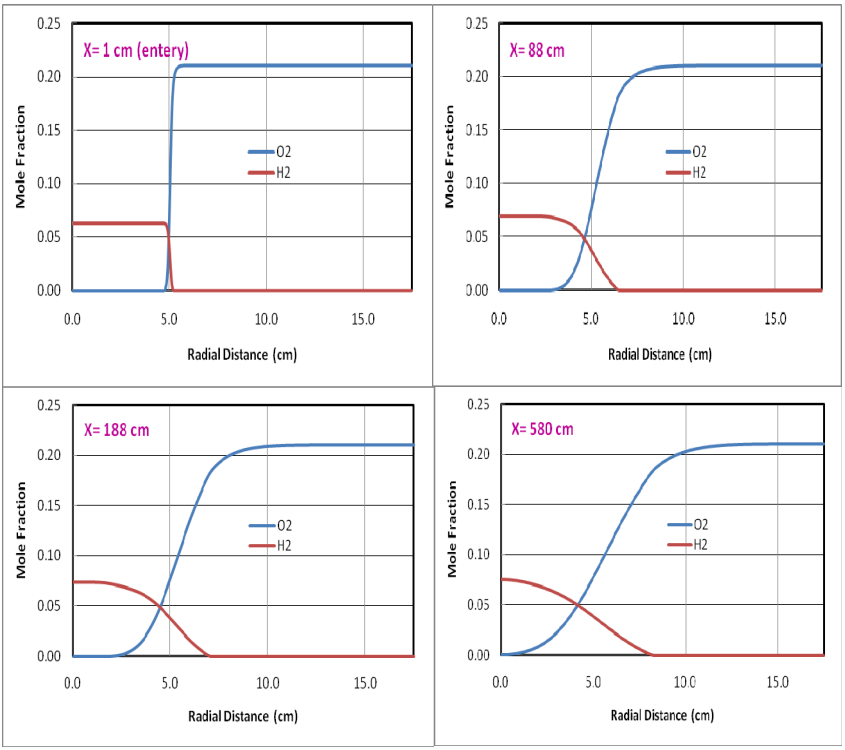

Figure 3: Radial profiles of O_2 and H_2 at different axial sections.

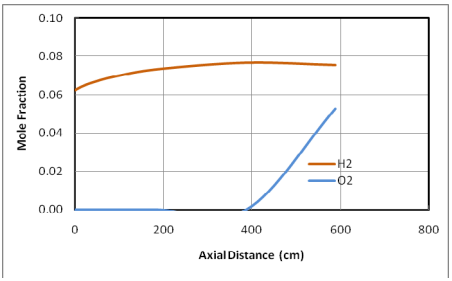

Figure 4: Axial distribution of H_2 and O_2 along the centerline of the reformer.

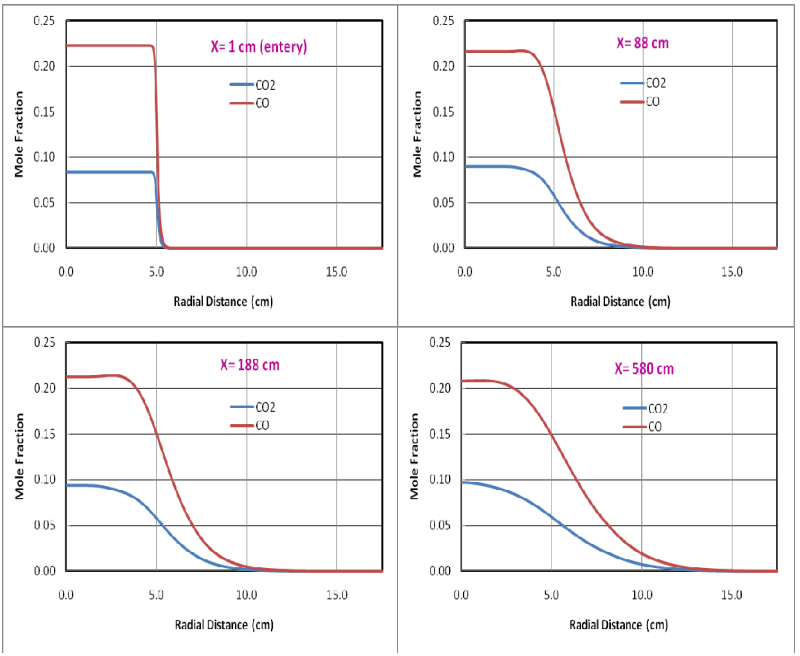

Figure 5: Radial profiles of CO_2 and CO at different axial sections.

where φ is the mole fraction of any gas, u is the axial velocity, ρ is the density and the integration is over the entire exit (from the centerline, r = 0, to the reformer wall $r = r_o$). Equation (7) is used to compute the average mole fraction of H_2. A value of 0.05 is as compared with the reported measured value of 0.0618 [10]. This discrepancy could be attributed to the dilution of hydrogen with the surrounding air and also to the kinetics of the reaction mechanism. Moreover, the experimental data was not specific about the location of the reported value whether it is a mean buck value or a centerline value.

Figure 5 depicts the radial profiles of the mole fractions of CO and CO_2 at the same axial sections mentioned earlier. The main jet gases spread latterly as expected up to the exit section of the reformer as shown in Fig. 5. The axial

distributions of CO and CO_2 mole fractions, plotted in Fig. 6, show the expected increase in carbon dioxide in the expense of carbon monoxide. The average mole fraction of CO_2 is also calculated using Equation (7) to give a value of 0.06 which is much lower than that obtained experimentally (0.116). Moreover, the centerline value of the predicted CO_2 mole fraction is approximately 0.1. Should the data was taken at the reformer centerline then the above value is in good agreement with the experimental data. However, the predicted average mole fraction of CO is 0.141 which is in good agreement with the measure value of 0.139.

The predicted radial profiles of the mole fraction of CH_4 are illustrated in Fig. 7. Its axial distributions are shown in Fig. 8. It should be noted that the peaks that appears in the profiles of the mole fraction of CH_4 at the different axial sections, occur at the interface between the gasified gases (main jet) and the

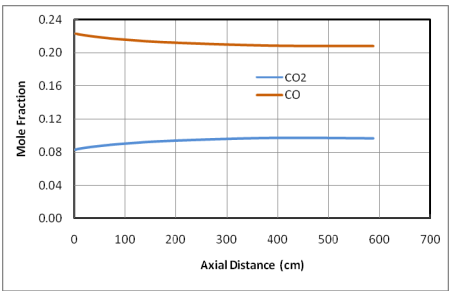

Figure 6: Axial distribution of CO_2 and CO along the centerline of the reformer.

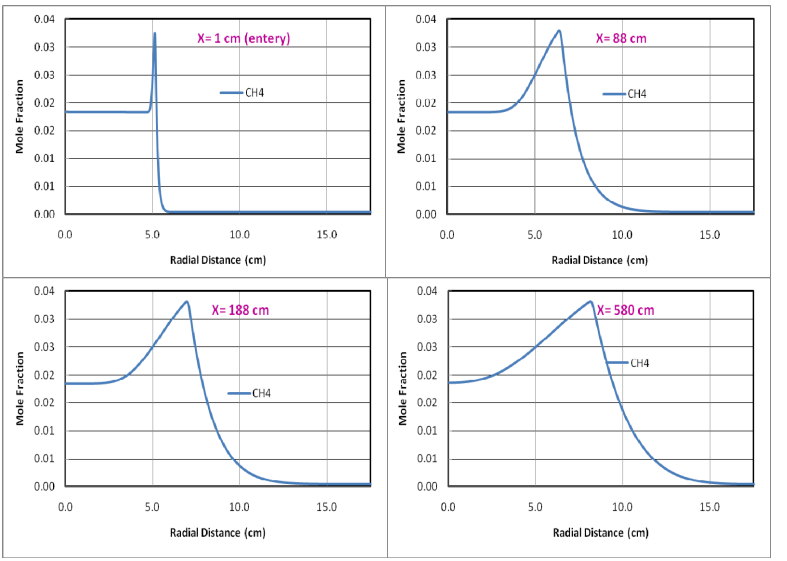

Figure 7: Radial profiles of CH_4 at different axial sections.

surrounding hot air. It becomes wider as we move towards the exit of the reformer. These peaks could possibly be due to the reactions involving generation and consumption of CH, CH_2 and CH_3.

The Averaged mole fraction of CH_4 is identical to the measured value of 0.025. Moreover, the computed mole fraction of nitrogen value of 0.606 is very close to the measured value of 0.586 [4].

Finally, the radial and axial profiles of temperature are plotted in Figs. 9-10. The spread of the main jet temperature in both axial and radial directions are quite obvious from the figures.

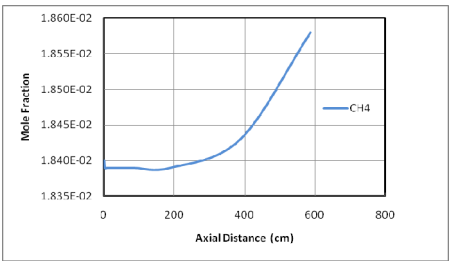

Figure 8: Axial distribution of CH4 along the centerline of the reformer.

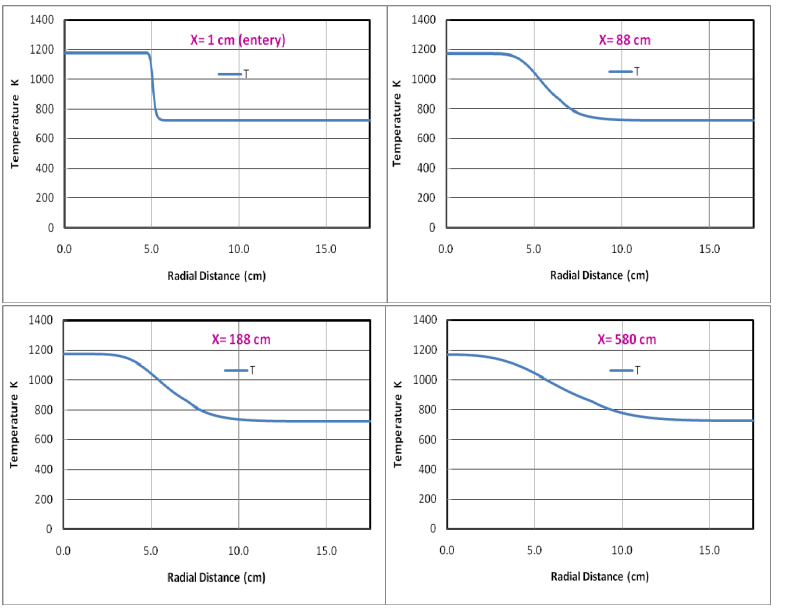

Figure 9: Radial profiles of the temperature at different axial sections.

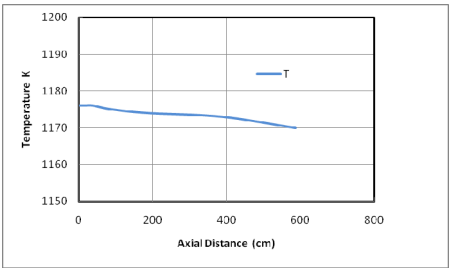

Figure 10: Axial distribution of the temperature along the centerline of the reformer.

5 Conclusions

The present work is concerned with the numerical computations of flow, heat transfer and chemical reactions in two-dimensional cylindrical gas reformers which is utilized to transform the chicken-manure, temperature-decomposed gas into useful fuel. The governing equations of momentum, mass continuity, energy, and species mass fractions are solved numerically in a finite-volume manner using a mesh of 300x1000 grid nodes in radial and axial directions respectively. The obtained results for the gas reformer in the form of mole fractions of the different gases, temperature and velocity are presented both axially (at centerline) and in the radial direction (at some specified axial locations). The average mole fractions of the gases exiting the reformer are compared with the limited available experimental data for similar reformers. The agreement is fairly good for all species expect for H_2 and CO_2. Some discrepancies in the computed values of H_2 and CO_2 are noticed. These discrepancies can be attributed to the lack of some information regarding the experimental data.

References

[1] Reardon, J.P., Lilley, A., Browne, K., Beard, K., Wimberly, J., and Avens, J., "Demonstration of a Small Modular Biopower System Using Poultry Litter," Final Report Department of Energy, 2001.

[2] Kirubakaran, V., Sivaramakrishnan, V., Premalatha, M. and Subramanian, P., "Establishing Auto-Gasification of Poultry Litter Using Thermogravimetric Analysis", Advances in Energy Research, (AER- 2006)

[3] Joseph, R.V. Flora, P.E. and Cyrus Riahi-Nezhad, "Availability of Poultry Manure as a Potential Bio-Fuel Feedstock for Energy Production", Final Report, South Carolina Energy Office, 2006.

[4] Yoshikawa, K. and Hara, T, "Long-term Operation of a Small-scale Gasification and Power Generation Plant for Chicken Manure", Abu Dhabi, U.A.E, Nov. 2008.

[5] Yoshikawa, K, "R&D (Research and Development) on Distributed Power Generation from Solid Fuels," Energy, Vol.31 (2006), pp.1656-1665.
[6] Min, T. and Yoshikawa, K., "Performance Demonstration of Dual-fueled Diesel Engine Combined with a Gasifier of Solid Wastes," Proc. 23rd International Conference on Incineration and Thermal Treatment Technologies, Phoenix, AZ, May, 2004.
[7] Tong, T.W., Abou-Ellail, M.M., Li, Y. and Beshay, K.R, 2004, Numerical Computation of Reacting Flow in Porous Burners with an Extended CH4 – Air Reaction Mechanism, Proceedings of HTFED04, 2004 ASME Heat Transfer/Fluids Engineering Summer Conference, July 11-15, Charlotte, NC, Paper # HT-FED 2004-56012.
[8] Abou-Ellail, M.M., Gosman, A.D., Lockwood, F.C. and Megahed, I.E.A., 1978, Description and Validation of a Three-Dimensional Procedure for Combustion Chamber Flows, AIAA Journal of Energy, 2, 71-80. Also, published in Turbulent Combustion, Ed. L. Kennedy, AIAA, 58, 163-190.
[9] Fiveland, W.A., 1982, "A Discrete-Ordinates Method for Predicting Radiative Heat transfer in Axisymmetric Enclosure", ASME Paper No. 82-HT-20.
[10] Yoshikawa, K., Private communications, 2009